Water Practice & Technology

IWA PUBLISHING

Water Practice & Technology Vol 17 No 5, 1113 doi: 10.2166/wpt.2022.054

Malachite green removal using ionic flocculation

Y. N. Teixeira [a,*], R. P. F. Melo[b], M. R. Fernandes[c], S. K. S. Carmo[b] and E. L. Barros Neto[d]

[a] Science and Technology Center, Federal University of Cariri (UFCA), Juazeiro do Norte CE, Brazil
[b] Department of Exact and Natural Sciences, Federal University of Semi-Árido (UFERSA), Mossoró, RN, Brazil
[c] Department of Engineering and Technology, Federal University of Semi-Árido (UFERSA), Mossoró, RN, Brazil
[d] Department of Petroleum Engineering, Federal University of Rio Grande do Norte (UFRN), Natal, RN, Brazil
*Corresponding Author. E-mail: yago.neco.teixeira@hotmail.com

YNT, 0000-0002-1538-4655

ABSTRACT

The use of ionic flocculation is proposed to remove malachite green (MG), in this case, from water. A surfactant with the polluted solution and calcium is added. The surfactant-calcium reaction forms a precipitate, which aggregates into flocs on agitation. The flocs adsorb MG, which can then be removed by centrifugation. Ionic flocculation was assessed by varying parameters including: surfactant and MG concentrations, electrolyte content, pH, contact time, etc. The isotherm and adsorption kinetic models that best fit this process are the Langmuir and pseudo-second-order models, respectively. MG removal efficiency of 96% was obtained at pH 9, with surfactant concentration 1,400 mg L^{-1}, MG concentration 10 mg L^{-1} and contact time 10 minutes. The process has potential for pollutant removal.

Key words: adsorption, ionic flocculation, isotherms, kinetics, malachite green, surfactant

HIGHLIGHTS

- Surfactant-based vegetable fat removes malachite green.
- Ionic flocculation is a fast process.
- Equilibrium quickly reached.
- Physicochemical analysis of post-process effluent.
- Malachite green removal efficiency up to 96%.

GRAPHICAL ABSTRACT

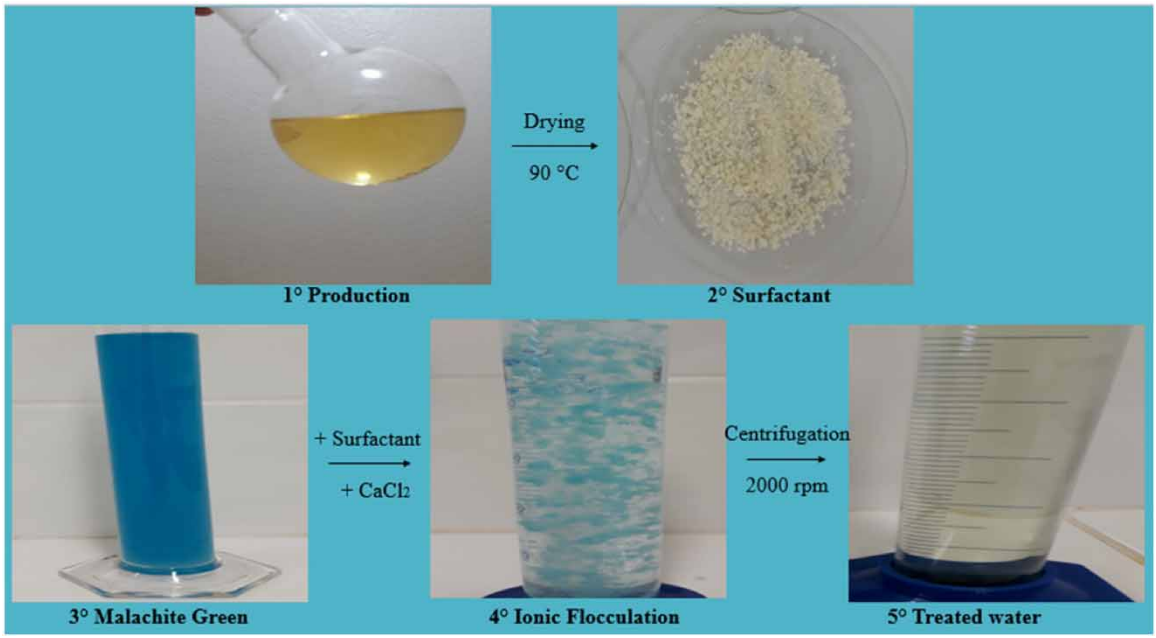

INTRODUCTION

The textile, paper and cellulose, cosmetic and food industries use more than 10,000 types of dyes, resulting in large amounts and variability of colored effluents (Dahri *et al.* 2014).

Malachite green (MG) is a toxic cationic dye, widely used to dye silk, cotton, wool, wood and leather. It is also used as an antibacterial agent and fungicide in fish farming, aquaculture and animal breeding due to its efficacy and low cost (Oyelude *et al.* 2018; Xie *et al.* 2020). However, many hostile effects such as carcinogenicity, mutagenesis and malformation have been related to different organisms, especially mammals (Srivastava *et al.* 2004). The use of MG in aquaculture companies is prohibited in several countries and its tolerance limit in water bodies was established at a concentration of 0.5–100 μg L^{-1} (Zhang *et al.* 2017). Thus, specific monitoring of MG consumption and its removal from industrial wastewater should be considered, due to its extensive destructive effects on the environment and health of fish and mammals (Salamat *et al.* 2019).

The techniques used in wastewater treatment include: coagulation-flocculation (Albuquerque *et al.* 2013), advanced oxidation processes (Karthikeyan *et al.* 2011), nanofiltration (Gozálvez-Zafrilla *et al.* 2008), photocatalysis (Das & Dhar 2020) and adsorption (Mahanta *et al.* 2009). Adsorption has been used widely, relative to other techniques, for its simplicity, facility and high efficiency (Wong *et al.* 2003).

Several types of adsorbents have been tested for their capacity to remove dyes from effluents – e.g., silica gel (Andrzejewska *et al.* 2007), alumina (Adak *et al.* 2005), zeolites (Alver & Metin 2012) and modified chitosan (Sadiq *et al.* 2020). With respect to MG removal, the adsorbents tested include magnetic microspheres (Pan *et al.* 2019), microplastics (Lin *et al.* 2020), activated carbon (Qu *et al.* 2019) and carbon composites (Adebayo *et al.* 2020).

Surfactants were tested as separation agents in a number of processes, such as cloud point extraction (Melo *et al.* 2014), microemulsion (Beltrame *et al.* 2005) and micellar ultrafiltration (Ahmad *et al.* 2006). Another promising process is ionic flocculation, in which low-cost surfactants are used. Amphiphilic surfactants are easily obtained by the saponification reaction between plant and animals fats, and a strong base. In aqueous media, these surfactants react with calcium ions, forming surfactant flocs. Their polar-nonpolar characteristics make them useful for ionic flocculation because they can adsorb organic compounds (Melo *et al.* 2017). The use of ionic flocculation is proposed in this study to remove MG from a synthetic textile effluent.

METHODS

Surfactant production

The surfactant used was synthesized in the laboratory from industrialized sunflower oil and sodium hydroxide p.a. by saponification, with mass proportions of 55.55 and 44.45%, respectively. The sunflower oil (10 g) and NaOH (8 g) were diluted in 90 mL of ethyl alcohol and 40 mL of distilled water, respectively. The resulting solutions were mixed and then heated. An Allihn condenser was used for alcohol reflux during the 90-minute saponification process. After saponification, the alcohol and water were evaporated to collect the surfactant formed. The surfactant was dried at 90 °C for 120 minutes.

Ionic flocculation tests

The MG-contaminated effluent was prepared at 120 mg L^{-1}. Next, the surfactant and $CaCl_2$ were weighed to obtain the desired surfactant concentration in 50 mL of the effluent. The $CaCl_2$ was weighed so that the calcium ion concentration in solution was half the surfactant concentration. This proportionality has little effect on process efficiency (Cavalcante *et al.* 2018).

The surfactant was dissolved totally in the effluent solution, which was agitated at 20 rpm, and the pH adjusted to 9. The $CaCl_2$ was always added after complete dissolution of the surfactant and pH adjustment. The $CaCl_2$ addition causes surfactant precipitation and floc formation. The resulting combined system was agitated for 5 minutes at 20 rpm to help the interaction between surfactant flocs and MG, promoting pollutant adsorption on the floc surface.

The final solution was centrifuged at 2,000 rpm for 5 minutes in an OEM/Unbranded 80-2B tabletop centrifuge, to separate the flocs from the solution. Solution samples were analyzed using a Gehaka UV-340G spectrophotometer (617 nm) to determine the effluent's final pollutant concentration. The amounts of MG adsorbed over time and in equilibrium were determined using Equations (1) and (2), respectively:

$$q_t = \frac{C_o - C_t}{m} V \tag{1}$$

$$q_e = \frac{C_o - C_e}{m} V \tag{2}$$

where C_o is the initial MG concentration (mg L^{-1}), C_t the MG concentration at time t (mg L^{-1}), C_e the MG concentration in equilibrium (mg L^{-1}), m the weight of surfactant used (g), V the solution volume (L), q_t the amount of MG adsorbed over time t (mg of dye/g of adsorbent), and q_e the amount of MG adsorbed in equilibrium (mg of dye/g of adsorbent).

Test regimes used

Table 1 summarizes the tests performed (adsorbent dosage, dye concentration, contact time, influence of pH and influence of electrolytes).

A concentration of 10 mg-MG L^{-1} was selected as the standard dose for the adsorbate because it exceeds the MG tolerance limit in water bodies (Zhang *et al.* 2017). In the MG concentration variation study, the highest MG concentration was 120 mg L^{-1}, which is significantly higher than that of the dyes present in textile effluents (Sirianuntapiboon *et al.* 2007).

To analyze contact time, the surfactant was dissolved in the effluent, pH adjusted (to 9) and $CaCl_2$ added. In assessing the effect of pH, the pH was adjusted after adding the surfactant and before adding $CaCl_2$. The influence of electrolytes was investigated because textile effluents have high electrolyte concentrations, mainly sodium chloride (NaCl) and sodium sulphate (Na_2SO_4) (Hunger 2003; Verma *et al.* 2012).

Adsorption kinetics

For MG's adsorption kinetics, the surfactant concentration and effluent volume were maintained at 1,400 mg L^{-1} and 50 mL, respectively, with MG concentrations of 10, 20, 40, 60, 80 and 120 mg L^{-1}. The residual MG concentration after flocculation and centrifugation was analyzed using a UV-Vis spectrophotometer. The experimental data were fitted to the pseudo-first order, pseudo-second order, Elovich and intraparticle diffusion models – see

Table 1 | Test regimes

Test	Surfactant concentration (mg L^{-1})	MG concentration (mg L^{-1})	NaCl concentration (mol L^{-1})	Time (min)	pH	Temperature (°C)	Volume (mL)
Adsorbent dosage	500–2,000 (increments 100 mg L^{-1})	10	0	10	9	25	50
MG concentration	1,400	10, 20, 40, 60, 80, 120	0	120	9	25	50
Contact time	1,400	10, 20, 40, 60, 80, 120	0	10, 30, 60, 90, 120, 150, 180, 210	9	25	50
pH	1,400	10	0	10	7, 8, 9, 10, 11, 12, 12.7	25	50
Electrolytes	1,400	10	0.02, 0.08, 0.1, 0.15, 0.2, 0.3, 0.4, 0.6, 0.8, 1	10	9	25	50

Equations (3)–(6) below, respectively:

$$q_t = q_e(1 - e^{-k_1 t}) \tag{3}$$

$$q_t = \frac{q_e^2 k_2 t}{1 + q_e k_2 t} \tag{4}$$

$$q_t = \frac{1}{\beta}\ln(1 + \alpha\beta t) \tag{5}$$

$$q_t = K_d t^{0.5} + C \tag{6}$$

where k_1 is the pseudo-first-order adsorption rate constant (min^{-1}), k_2 the pseudo-second-order adsorption rate constant (g mg^{-1} min^{-1}), α the constant related to the initial adsorption rate (mg g^{-1} min^{-1}), β the desorption constant (mg g^{-1}), K_d the intraparticle diffusion coefficient (mg g^{-1} $min^{-0.5}$), C the constant related to diffusion resistance (mg g^{-1}) and t the time (min).

Adsorption equilibrium

Four theoretical adsorption isotherm models – Freundlich, Langmuir, Temkin and Dubinin-Radushkevich (DR) – were used to describe the equilibrium between MG and the surfactants' adsorbent surface.

The Freundlich model represents adsorption in heterogeneous systems, with multilayer generation, and is represented by Equation (7):

$$q_e = k_F C_e^{1/n} \tag{7}$$

where k_F is the Freundlich adsorption capacity constant (L mg^{-1}) and n the constant related to surface heterogeneity.

The Langmuir model selected occurs on homogeneous surfaces and in monolayers. Because of this, this model makes it possible to calculate the maximum adsorption capacity on the adsorbent surface (White *et al.* 2018). The Langmuir model is represented by Equation (8):

$$q_e = \frac{q_{max} k_L C_e}{1 + k_L C_e} \tag{8}$$

where $q_{máx}$ is the maximum adsorption capacity (mg g^{-1}) and k_L the adsorbate/adsorbent interaction constant (L mg^{-1}), also related to adsorption heat (Romero-Cano *et al.* 2017). The Langmuir model can also be used to calculate the separation factor (R_L), that is, the degree of development of the adsorption process. R_L can be calculated using Equation (9). Table 2 shows the interpretation of this parameter (Mahmoud *et al.* 2017).

Table 2 | Langmuir isotherm separation factor

R_L	Behavior
$R_L = 0$	Irreversible
$0 < R_L < 1$	Favorable
$R_L = 1$	Linear
$R_L > 1$	Unfavorable

$$R_L = \frac{1}{1 + K_L Co} \tag{9}$$

The Temkin model describes adsorption considering the adsorbate-adsorbent interactions and the uniform distribution of activation energies. It is assumed that the adsorption energy of the molecules in the layer tends to decrease linearly with increasing adsorbent cover (Abdelnaeim *et al.* 2016). The Temkin model is represented by Equation (10):

$$q_e = \frac{RT}{b} \ln(k_T C_e) \tag{10}$$

where k_T is the model constant (L g^{-1}), b the Temkin constant related to adsorption energy (J mol^{-1}), R the gas constant (8.3145 J mol^{-1} K^{-1}) and T the temperature at which the process occurred (298.15 K).

The DR model – represented by Equation (11) – describes adsorption on non-homogeneous surfaces with pore filling, considering Gaussian distribution of the heterogeneous surface and energy (Inyinbor *et al.* 2016).

$$q_e = q_{mâx} \exp\left\{-k_{DR}\left[RTln\left(1 + \frac{1}{C_e}\right)\right]^2\right\} \tag{11}$$

where k_{DR} is the model constant associated with adsorption energy (mol^2 kJ^{-2}).

The average adsorption energy can be calculated by Equation (12):

$$E = \frac{1}{\sqrt{2k_{DR}}} \tag{12}$$

where E is the average adsorption energy (kJ mol^{-1}). The value of E can be used to assess the nature of the process: physical adsorption ($E < 8$ kJ mol^{-1}), ionic exchange ($8 < E < 16$ kJ mol^{-1}) or chemical adsorption ($E >$ 16 kJ mol^{-1}) (Kaveeshwar *et al.* 2018).

Removal efficiency

MG removal efficiency was calculated by Equation (13):

$$\%Efficiency = \left(\frac{C_o - C_e}{C_o}\right) 100 \tag{13}$$

Error analysis

The kinetic models and equilibrium isotherms were validated using Equation (14) to calculate the sum of the squared errors (SSE).

$$\sum_{i=1}^{n} (q_{exp} - q_{calc})_i^2 \tag{14}$$

where q_{exp} and q_{calc} are the experimental and predicted values, respectively. SSE is widely applied in adsorption studies and adequate for high concentration data (Nascimento *et al.* 2020).

Physicochemical analysis of the effluent treated

Treated waters were analyzed to find suitable disposal destinations. Two types were analyzed, with (A1) and without (A2) NaCl added. The parameters determined were: pH, electrical conductivity (EC), potassium (K^+), sodium (Na^+), calcium (Ca^{2+}), magnesium (Mg^{2+}), free chlorine (Cl), carbonate (CO_3^{2-}), bicarbonate (HCO_3^-), sodium adsorption ratio (SAR) and hardness.

RESULTS AND DISCUSSION

Adsorbent dosage

Figure 1 shows the effect of surfactant dosage on MG removal.

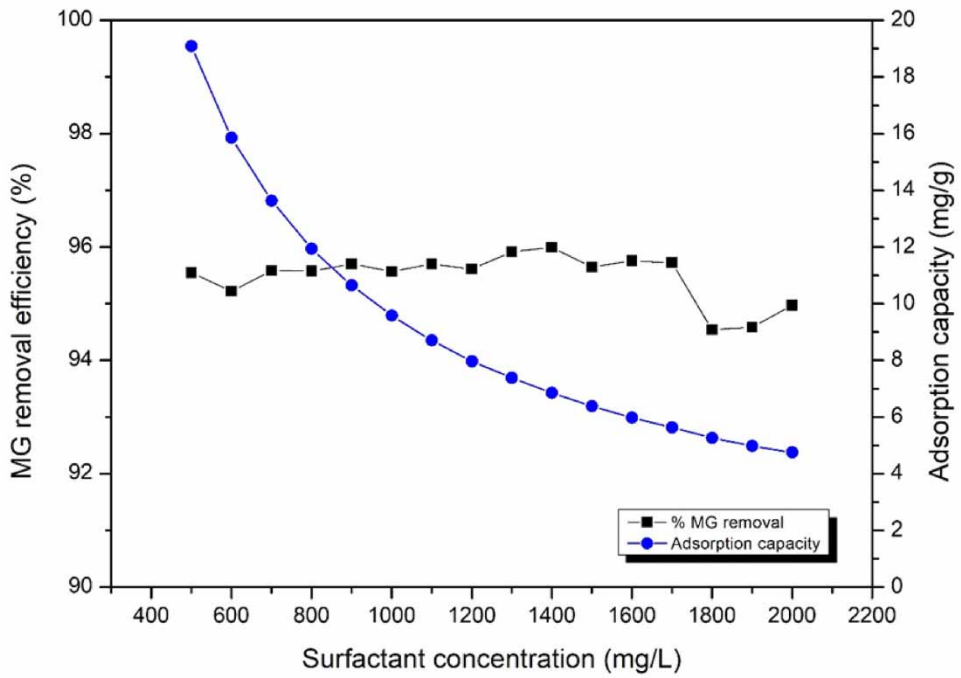

Figure 1 | Effect of surfactant dosage on MG removal efficiency and adsorption capacity (10 mg-MG L^{-1}, 50 mL of solution, pH 9, 25 °C).

Within the surfactant dosage range studied, MG removal efficiency was not altered significantly by variation in surfactant concentration – i.e., ionic flocculation is independent of surfactant dosage. The high removal efficiency can be explained by the large number of adsorption sites available and interaction between MG and the hydrophobic part of the surfactant.

The MG-adsorption capacity declined significantly with increasing surfactant dosage. The greatest adsorption capacity (19.09 mg g^{-1}) was for a surfactant concentration of 500 mg L^{-1} and the lowest (4.75 mg g^{-1}) for 2,000 mg L^{-1}. This decline may be due to the ready availability of adsorption sites leading to competition for MG molecules and the accumulation of unsaturated adsorbent particles reducing the surface area (Ozacar & Sengil 2005; Ramesh *et al.* 2008). The increased surfactant concentration is also insufficient to promote MG

removal, as the latter's concentration in solution is very low, even when a small amount of surfactant is used (500 mg L^{-1}). Eltaweil *et al.* (2020) used a mesoporous magnetic biochar composite to adsorb MG, and Salamat *et al.* (2019) used nanochitosan prepared from shrimp shells, obtaining similar results.

The process is infeasible with surfactant concentrations below 500 mg L^{-1}, as there is not enough surfactant to produce flocs large enough for separation by centrifugation. The optimal surfactant concentration was 1,400 mg L^{-1}, with approximately 96% removal efficiency.

Dye concentration

Figure 2 presents the effect of initial MG concentration (10–120 mg L^{-1}) on surfactant adsorption capacity at 10 minutes contact time.

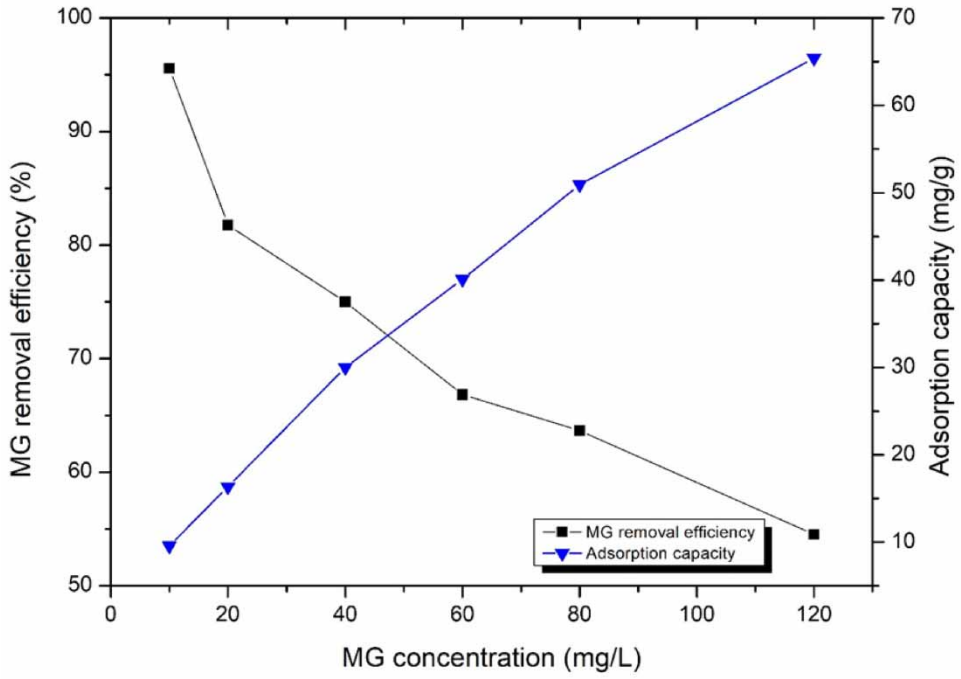

Figure 2 | Effect of MG concentration on removal efficiency and adsorption capacity (1400 mg L^{-1} of surfactant, 50 mL of solution, pH 9, 25 °C).

As the initial MG concentration was increased from 10 to 120 mg L^{-1}, MG removal efficiency declined from 96 to 55%. The higher removal efficiency at low dye concentrations may be attributed to the greater proportional availability of active adsorbent sites. However, with increased dye concentration, active surfactant sites become saturated, resulting in decreased efficiency (Verma *et al.* 2020).

With respect to adsorption capacity, it rose from 9.6 mg g^{-1} in 10 mg L^{-1} dye solution to 65 mg g^{-1} in 120 mg L^{-1} of solution – i.e., as the initial MG concentration increased. This increase can be attributed to the larger number of MG molecules in solution. Thus, capacity rises until equilibrium time and maximum adsorption capacity are reached.

Contact time

Figure 3 shows the effect of contact time on MG removal efficiency, and the influence of equilibrium time on MG removal.

Figure 3 shows that process equilibrium is achieved in only 10 minutes at 10 mg-MG L^{-1} concentration. At higher MG concentrations, equilibrium is reached in 120 minutes. For example, for 60 mg-MG L^{-1} concentration, MG removal is 67% and adsorption capacity 40 mg g^{-1} at 10 minutes; after 120 minutes, MG removal and adsorption capacity become constant (98% and 59 mg g^{-1}).

The MG adsorption capacity increases over time due to the availability of active adsorption sites. However, when equilibrium is reached, adsorbent saturation keeps adsorption capacity and removal efficiency constant.

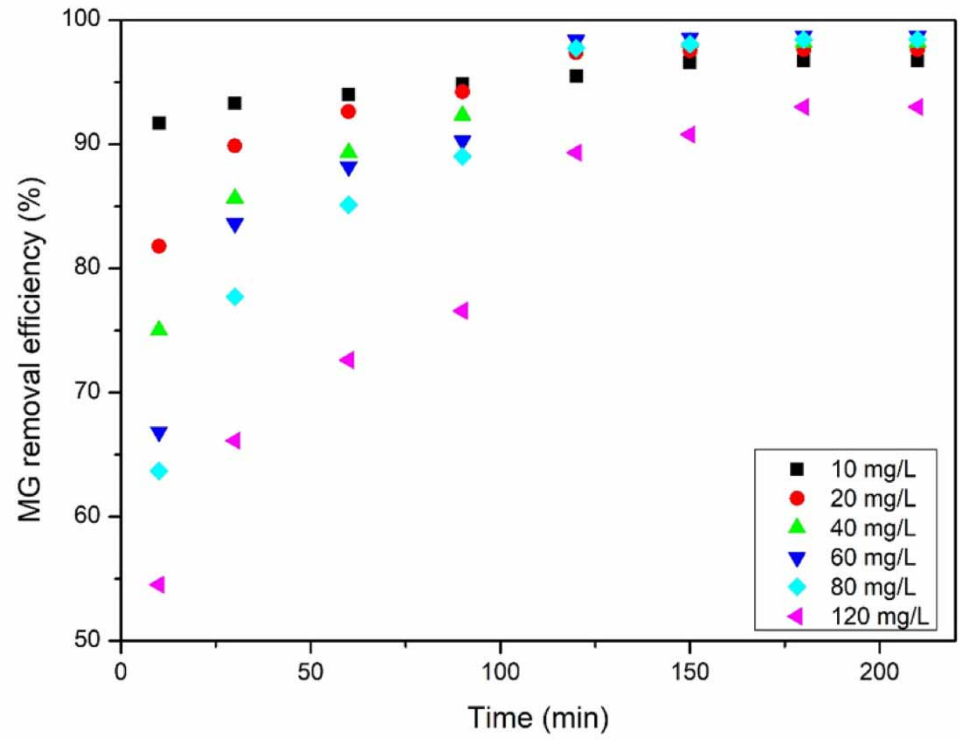

Figure 3 | Effect of equilibrium time on MG removal (1,400 mg L^{-1} of surfactant, 50 mL of solution, pH 9, 25 °C).

Khawaja *et al.* (2021) used copper and graphene oxide nanoparticles with cellulose for MG adsorption, obtaining similar results.

Kinetics and adsorption modeling

Adsorption kinetics were studied to investigate the effects of contact time and obtain results for adsorption kinetic model parameters. The best fit among the kinetic models was assessed using the coefficient of determination (R^2) and SSE. Figure 4 and Table 3 present the adsorption behavior results for different MG concentrations in the different kinetic models.

Table 3 shows that the pseudo-second-order model gave the best adsorption kinetics fit for the different MG concentrations – i.e., it exhibited the highest R^2 and lowest SSE values.

The pseudo-first-order and Elovich models yielded calculated values close to their theoretical counterparts, as well as high R^2 (Elovich model) and very high SSE (both). Similar results have been reported by others, e.g., in the use of nanocomposites for MG adsorption (Rajabi *et al.* 2019), MG adsorption by copper oxide-loaded, activated carbon (Sharifpour *et al.* 2019), MG removal by polyurethane functionalized by salicylate (El-Bouraie 2015) and MG adsorption in a polyamide nanocomposite containing ceric oxide as the adsorbent (Ghanbary & Jafarnejad 2017).

Adsorption mechanism

To assess the adsorption mechanism, the intraparticle diffusion model was analyzed based on the adsorption kinetic results. Figure 5 and Table 4 depict the results of the adsorption mechanism for different MG concentrations.

Figure 5 shows that MG adsorption onto the surfactant follows a two-stage mechanism ($K_{d,1} > K_{d,2}$). The first is related to external surface adsorption, that is, rapid diffusion of MG molecules on the adsorbent's outer surface until saturation. In the second stage, the effect of intraparticle diffusion decreases significantly at all concentrations, meaning that adsorption equilibrium was reached at this stage through the adhesion of MG molecules inside the surfactant flocs (attached to the hydrophobic tail of the surfactant) (Wu *et al.* 2005; Mohammed *et al.* 2015).

The estimated constants associated with boundary-layer thickness (C) increased in both stages, indicating increases in the boundary-layers' effects on the process at each stage. Values of C exceeding 0 also suggest that another mechanism, such as film diffusion, was involved as an adsorption rate-limiting step in conjunction with pore diffusion in the adsorption mechanism (Weber 1984).

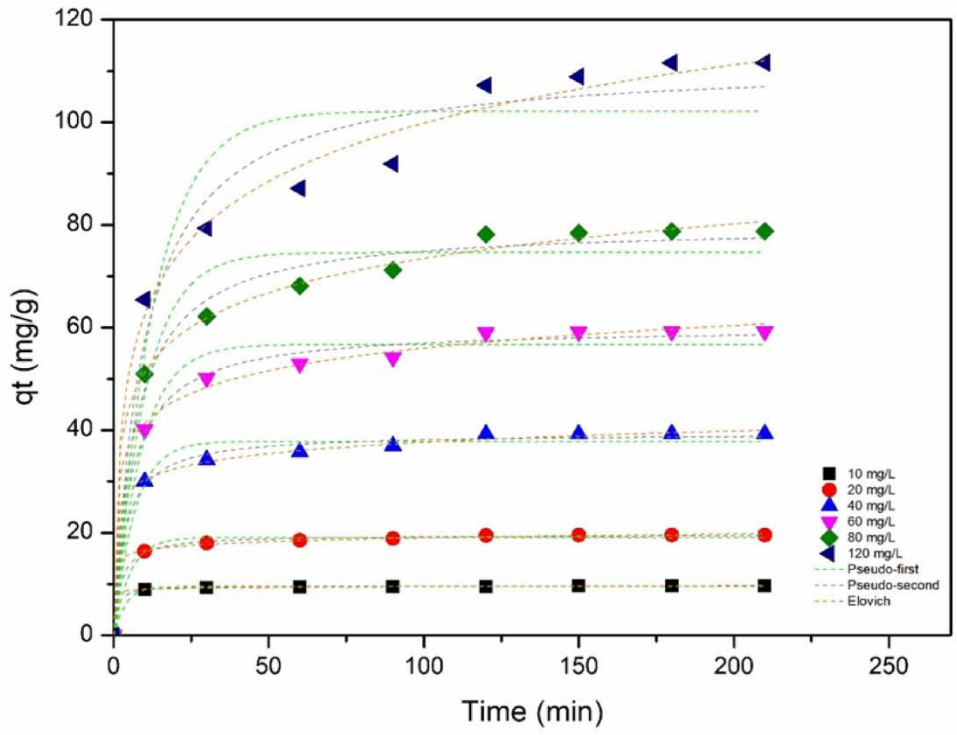

Figure 4 | Pseudo-first and second order, and Elovich kinetic models (1,400 mg L^{-1} of surfactant, 50 mL of solution, pH 9, 25 °C).

Table 3 | Adsorption kinetic model parameters

	Concentration (mg L^{-1})					
Kinetic models and parameters	**10**	**20**	**40**	**60**	**80**	**120**
$q_{e,\ exp}$ (mg g^{-1})	9.67	19.52	39.29	59.24	78.75	111.59
Pseudo-first order						
K_1 (min^{-1})	0.09	0.07	0.07	0.07	0.07	0.07
$q_{e,\ calc}$ (mg g^{-1})	20.58	17.03	46.28	84.63	132.87	263.88
R^2	0.64	0.77	0.79	0.69	0.64	0.54
SSE	165.21	54.64	57.77	92.18	111.35	161.38
Pseudo-second order						
K_2 (g mg^{-1} min^{-1})	0.30	0.02	6.60×10^{-3}	3.20×10^{-3}	1.90×10^{-3}	8.00×10^{-4}
$q_{e,\ calc}$ (mg g^{-1})	9.71	19.72	39.95	60.57	81.04	115.87
R^2	0.99	0.99	0.99	0.99	0.99	0.99
SSE	0.05	0.03	0.028	0.02	0.02	0.030
Elovich model						
α (mg g^{-1} min^{-1})	1.07×10^{14}	6.72×10^{5}	4,410	431	195	75.71
β (mg g^{-1})	4.02	0.94	0.31	0.16	0.10	0.06
R^2	0.96	0.96	0.97	0.95	0.97	0.94
SSE	0.02	0.28	2.23	12.50	15.44	98.41

The plot of q_t *vs* $t^{0.5}$ did not cross the origin at any MG concentration. Intraparticle diffusion was, thus, not the only adsorption rate-limiting step and different adsorption mechanisms may be occurring simultaneously (Kumar *et al.* 2010). Li *et al.* (2021) obtained similar results using polyurethane plastic residues in MG dye adsorption.

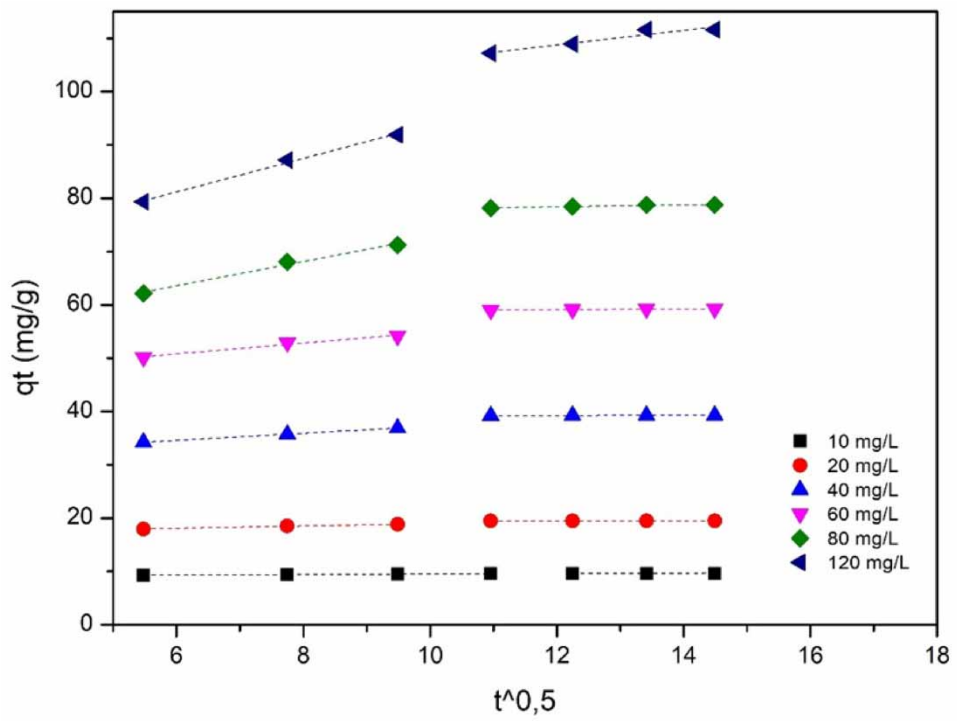

Figure 5 | Intraparticle diffusion model (1,400 mg-surfactant L^{-1}, 50 mL of solution, pH 9, 25 °C).

Table 4 | Intraparticle diffusion model parameters

		Intraparticle diffusion				
MG concentration (mg L^{-1})	$q_{e,\ exp}$ (mg g^{-1})	Stage	C (mg g^{-1})	Kd (mg g^{-1} $min^{-0.5}$)	R^2	SSE
10	9.67	I	9.10	0.04	0.99	0.01
		II	9.58	0.01	0.54	0.01
20	19.52	I	16.80	0.22	0.99	0.01
		II	19.33	0.01	0.81	0.01
40	39.29	I	30.61	0.66	0.99	0.01
		II	39.09	0.01	0.31	0.01
60	59.24	I	44.79	1.01	0.96	0.15
		II	58.34	0.06	0.87	0.01
80	78.75	I	49.95	2.27	0.98	0.45
		II	76.33	0.17	0.87	0.02
120	111.59	I	62.34	3.14	0.99	0.33
		II	92.42	1.36	0.87	1.18

Adsorption isotherms

Adsorption isotherms are important for understanding the adsorption mechanism by correlating equilibrium data with theoretical models, on which basis it is possible to describe how MG molecules interact with active surfactant sites (Demiral & Güngör 2016). Batch experiments were performed under standard conditions – surfactant 1,400 mg L^{-1}, MG concentration range 10 to $^{-}$120 mg L^{-1}, agitation 20 rpm for 120 minutes, and pH 9. Figure 6 and Table 5 present the MG adsorption behavior results for the different isotherm models.

Table 5 shows that the Langmuir model offers the best fit for the experimental data, with the lowest SSE value (177) and the highest R^2 (0.98). This indicates that MG molecules are adsorbed homogeneously at the active

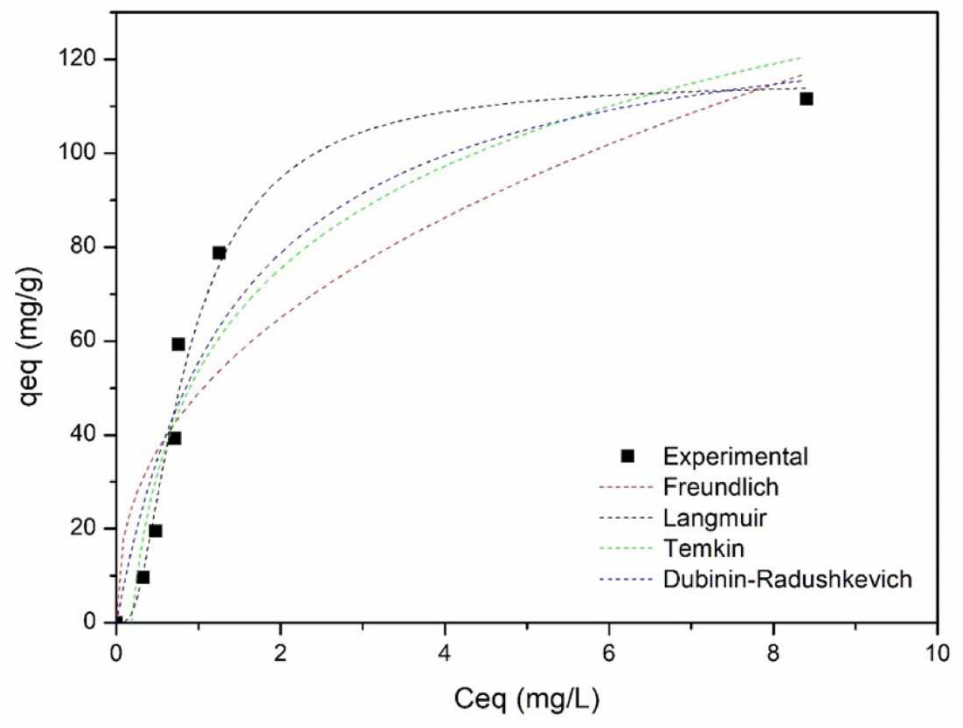

Figure 6 | Adsorption isotherm model and actual results.

Table 5 | Adsorption isotherm model parameters

Freundlich				Langmuir				
n	K_F (L mg^{-1})	R^2	SSE	$q_{máx}$ (mg g^{-1})	K_L (L mg^{-1})	R_L*	R^2	SSE
2.40	49	0.80	1,638	116	0.70	0.13	0.98	177
Temkin				**D-R**				
k_T (L mg^{-1})	b (J mol^{-1})	R^2	SSE	$q_{máx}$ (mg g^{-1})	k (mol^2 kJ^{-2})	E (kJ mol^{-1})	R^2	SSE
5.50	79	0.90	816	135	4.52*10^{-9}	10,518	0.90	886

*Calculated for initial concentration 10 mg-MG L^{-1}.

surfactant sites, and maximum adsorption capacity, q_{max}, of 116 mg g^{-1} is expected due to active site saturation. The separation factor, R_L, (0.13) indicates that MG separation by the surfactant is a favorable process ($0 < RL < 1$).

The low R^2 values for the Freundlich, Temkin and D-R models ($R^2 < 0.95$) and the highest SSE indicate that they do not fit the experimental data.

Thus, the Langmuir isotherm model represents this adsorption process – i.e., adsorption occurs in a monolayer and bond energies at the surfactant's active sites are equivalent, meaning that each MG molecule occupies only one adsorption site.

Effect of pH

The pH range was between 7 and 12.7. At pHs 7 and 8 an oil emulsion forms in water because the low pH converts the surfactant into its respective fatty acids, precluding floc formation due to the lack of carboxyl anions and making the process inviable (Melo *et al.* 2015). Figure 7 shows the MG adsorption behavior results for different pH values.

Without pH adjustment, the pH of samples containing only diluted surfactant is between 10 and 10.5, because of the reaction between fatty acids and NaOH. Figure 7 shows that varying the pH alone, without adding surfactant and/or calcium, may produce false results, as MG displays different colors for different pH intervals. The

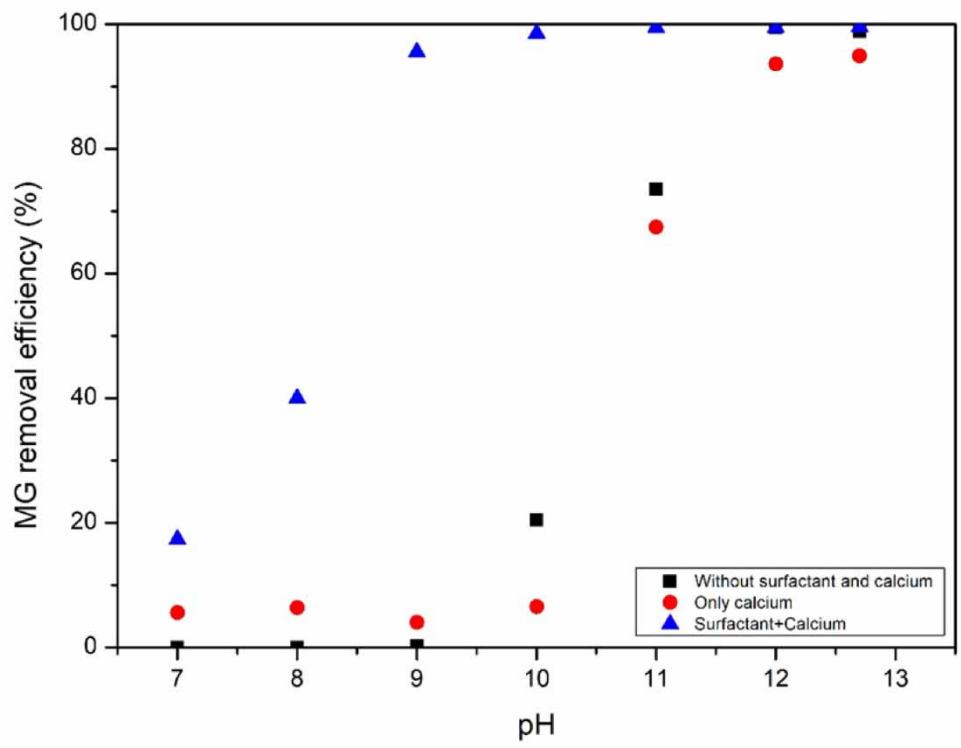

Figure 7 | Effect of pH on MG removal efficiency (1,400 mg-surfactant L^{-1}, 10 mg-MG L^{-1}, 50 mL of solution, 25 °C).

results were determined by UV-vis spectrophotometry, so the pH ranges in which MG maintains its natural color and in which it becomes colorless need study.

For pHs between 7 and 9, MG maintains its natural green color. With the addition of calcium alone, about 5% of the MG is removed by flocculation. Dye removal efficiency depends directly on the interaction between MG molecules and the surfactant's nonpolar tail. At pH values greater than or equal to 11, MG starts to become colorless, whether removed from the solution or not.

Thus, for analyses of MG removal efficiency by ionic flocculation, pH was initially corrected to pH 9 (within the range that does not produce false values). At pH 9, MG removal was 96%.

Effect of electrolytes

Figure 8 shows MG adsorption behavior for different NaCl concentrations, with fixed surfactant and dye concentrations.

Figure 8 shows that the presence of electrolytes lowers MG removal efficiency slightly. Removal efficiency was approximately 96% for samples without electrolyte addition, while in those containing 1 mol L^{-1} NaCl it was slightly more than 92%.

The electrolytes inhibit floc formation, as precipitation tolerance – i.e., the minimum calcium concentration capable of causing precipitation – rises when electrolyte concentration increases, because dissolved anionic monomers decline in the surfactant when NaCl is added (Noïk *et al.* 1987; Stellner & Scamehorn 1989).

Analysis of treated water

As noted previously, two types of water were analyzed: NaCl was added to A1 but not to A2 (Table 6).

The ideal values – data rows 3 and 6 in Table 6 – are taken from the University of California Committee of Consultants, of 1974. They are used to compare water analyses with irrigation needs (UCCC 1974). Table 6 shows that A1 water is not suitable for irrigation, since it is only within the ideal range with respect to HCO_3^-.

A2 water is fairly good for irrigation because it is only outside the ideal ranges for pH, Cl and hardness.

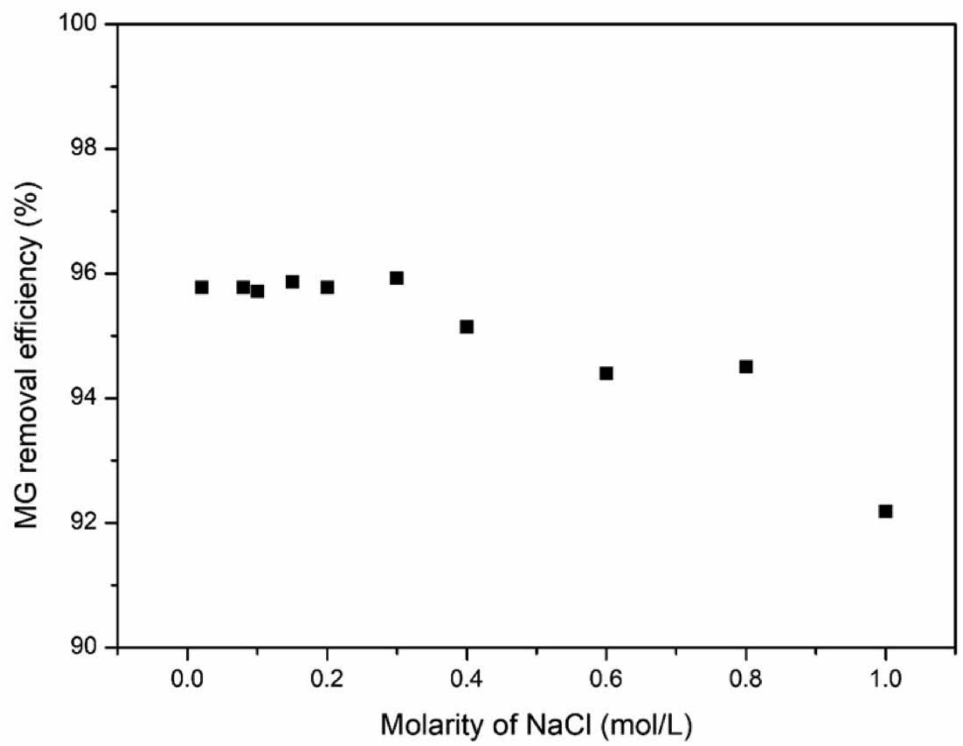

Figure 8 | Effect of electrolytes on MG removal efficiency (1,400 mg-surfactant L^{-1}, 10 mg-MG L^{-1}, 50 mL of solution, pH 9, 25 °C).

Table 6 | Post-treatment water analysis parameters

Identification	pH	CE (μS/cm)	K^+ (mmol/L)	Na^+ (mmol/L)	Ca^{2+} (mmol/L)	Mg^{2+} (mmol/L)	
A1	9.7	296,000	0.91	111.17	14.10	3	
A2	10.9	2,570	0.09	4.49	14.90	0.20	
Ideal	6.5–8.5	<3,000	–	0–9	–	–	
	CL (mmol/L)	**CO_3^{2-} (mmol/L)**	**HCO_3^- (mmol/L)**	**SAR**	**Hardness (mg-$CaCO_3$/L)**	**Cations (mmol/L)**	**Anions (mmol/L)**
A1	255	0.80	1.40	38	855	129.2	257.2
A2	19.20	0.80	1.90	1.6	755	19.7	21.9
Ideal	0–10	–	0–8.5	–	0–350	–	–

CONCLUSIONS

Ionic flocculation was used to remove MG from solution in this study.

- The surfactant-calcium combination has an MG removal efficiency of approximately 96% at 25 °C, with pH 9.
- With increasing dye concentration, surfactant adsorption efficiency tends to decline due to the saturation of active sites.
- Adding electrolytes to the effluent lowers adsorption efficiency a little.
- Equilibrium time is 10 minutes for 10 mg-MG L^{-1}, while, for concentrations above that, it is reached after 120 minutes.
- The Langmuir isotherm model best fits this adsorption process ($R^2 = 0.98$), with a separation factor (R_L) of 0.22.
- The pseudo-second-order kinetic model best fits the process.

The study's results demonstrate that ionic flocculation can be used to remove dyes from wastewater.

ETHICAL APPROVAL

Not applicable.

CONSENT TO PARTICIPATE AND PUBLISH

The authors confirm consent to publication and authorship of the study. Informed consent was obtained from all individual participants included in the manuscript.

COMPETING INTEREST

The authors declare that they have no known competing financial interests or personal relationships that could have appeared to influence the work reported in this paper.

DATA AVAILABILITY STATEMENT

All relevant data are included in the paper or its Supplementary Information.

REFERENCES

Abdelnaeim, M. Y., El Sherif, I. Y., Attia, A. A., Fathy, N. A. & El-Shahat, M. F. 2016 Impact of chemical activation on the adsorption performance of common reed towards Cu(II) and Cd (II). *International Journal of Mineral Processing* **157**, 80–88. https://doi.org/10.1016/j.minpro.2016.09.013.

Adak, A., Bandyopadhyay, M. & Pal, A. 2005 Removal of crystal violet dye from wastewater by surfactant-modified alumina. *Separation and Purification Technology* **44**(2), 139–144. https://doi.org/10.1016/j.seppur.2005.01.002.

Adebayo, M., Adebomi, J. I., Abe, T. O. & Areo, F. I. 2020 Removal of aqueous Congo red and malachite green using ackee apple seed-bentonite composite. *Colloid and Interface Science Communications* **38**, 100311. https://doi.org/10.1016/j.colcom.2020.100311.

Ahmad, A. L., Puasa, S. W. & Zulkali, M. M. D. 2006 Micellar-enhanced ultrafiltration for removal of reactive dyes from an aqueous solution. *Desalination* **191**(1–3), 153–161. https://doi.org/10.1016/j.desal.2005.07.022.

Albuquerque, L. F., Salgueiro, A. A., Melo, J. L. S. & Chiavone-Filho, O. 2013 Coagulation of indigo blue present in dyeing wastewater using a residual bittern. *Separation and Purification Technology* **104**, 246–249. http://dx.doi.org/10.1016/j.seppur.2012.12.005.

Alver, E. & Metin, A. U. 2012 Anionic dye removal from aqueous solutions using modified zeolite: adsorption kinetics and isotherm studies. *Chemical Engineering Journal* **200–202**, 59–67. https://doi.org/10.1016/j.cej.2012.06.038.

Andrzejewska, A., Krysztafkiewicz, A. & Jesionowski, T. 2007 Treatment of textile dye wastewater using modified silica. *Dyes and Pigments* **75**(1), 116–124. https://doi.org/10.1016/j.dyepig.2006.05.027.

Beltrame, L. T. C., Dantas Neto, A. A., Castro Dantas, T. N., Barros Neto, E. L. & Lima, F. F. S. 2005 Influence of cosurfactant in microemulsion systems for color removal from textile wastewater. *Journal of Chemical Technology & Biotechnology* **80**(1), 92–98. https://doi.org/10.1002/jctb.1162.

Cavalcante, P. R. M., Melo, R. P. F., Castro Dantas, T. N., Dantas Neto, A. A., Barros Neto, E. L. & Moura, M. C. P. A. 2018 Removal of phenol from aqueous medium using micellar solubilization followed by ionic flocculation. *Journal of Environmental Chemical Engineering* **6**(2), 2778–2784. https://doi.org/10.1016/j.jece.2018.04.025.

Dahri, M. K., Kooh, M. R. R. & Lim, L. B. L. 2014 Water remediation using low cost adsorbent walnut shell for removal of malachite green: equilibrium, kinetics, thermodynamic and regeneration studies. *Journal of Environmental Chemical Engineering* **2**(3), 1434–1444. https://doi.org/10.1016/j.jece.2014.07.008.

Das, K. C. & Dhar, S. S. 2020 Rapid catalytic degradation of malachite green by $MgFe_2O_4$ nanonparticles in presence of H_2O_2. *Journal of Alloys and Comounds* **828**, 154462. https://doi.org/10.1016/j.jallcom.2020.154462.

Demiral, H. & Güngör, C. 2016 Adsorption of copper (II) from aqueous solutions of activated carbon prepared from grape bagasse. *Journal of Cleaner Production* **124**, 103–113. https://doi.org/10.1016/j.jclepro.2016.02.084.

El-Bouraie, M. 2015 Removal of the malachite green (MG) dye from textile industrial wastewater using the polyurethane foam functionalized with salicylate. *Journal of Dispersion Science and Technology* **36**(9), 1228–1236. https://doi.org/10.1080/01932691.2014.964802.

Eltaweil, A. S., Mohamed, H. A., El-Monaem, E. M. A. & El-Subruiti, G. M. 2020 Mesoporous magnetic biochar composite for enhanced adsorption of malachite green dye: characterization, adsorption kinetics, thermodynamics and isotherms. *Advanced Powder Technology* **31**(3), 1253–1263. https://doi.org/10.1016/j.apt.2020.01.005.

Ghanbary, F. & Jafarnejad, E. 2017 Removal of malachite green from the aqueous solutions using polyimide nanocomposite containing cerium oxide as adsorbent. *Inorganic and Nano-Metal Chemistry* **47**(12), 1675–1681. https://doi.org/10.1080/24701556.2017.1357598.

Gozálvez-Zafrilla, J. M., Sanz-Escribano, D., Lora-García, J. & Hidalgo, M. C. L. 2008 Nanofiltration of secondary effluent for wastewater reuse in the textile industry. *Desalination* **222**(1–3), 272–279. https://doi.org/10.1016/j.desal.2007.01.173.

Hunger, K. 2003 *Industrial Dyes Chemistry, Properties, Applications*. Wiley-VHC, Germany.

Inyinbor, A. A., Adekola, F. A. & Olatunj, G. A. 2016 Kinetics, isotherms and thermodynamic modeling of the liquid phase adsorption of Rhodamine B dye on Raphia hookerie fruit epicarp. *Water Resources and Industry* **15**, 14–27. https://doi.org/10.1016/j.wri.2016.06.001.

Karthikeyan, K., Titus, A., Gnanamani, A., Mandal, A. B. & Sekaran, G. 2011 Treatment of textile wastewater by homogeneous and heterogeneous Fenton oxidation processes. *Desalination* **281**, 438–445. https://doi.org/10.1016/j.desal.2011.08.019.

Kaveeshwar, A., Revellame, E., Gang, D. D. & Subramaniam, R. 2018 Adsorption properties and mechanism of barium (II) and strontium (II) removal from fracking wastewater using pecan shell based activated carbon. *Journal of Cleaner Production* **193**, 1–13. https://doi.org/10.1016/j.jclepro.2018.05.041.

Khawaja, H., Zahir, E., Asghar, M. A. & Asghar, M. A. 2021 Graphene oxide decorated with cellulose and copper nanoparticle as an efficient adsorbent for the removal of malachite green. *International Journal of Biological Macromolecules* **167**, 23–34. https://doi.org/10.1016/j.ijbiomac.2020.11.137.

Kumar, P. S., Ramalingam, S. & Senthamarai, C. 2010 Adsorption of dye from aqueous solution by cashew nut shell: studies on equilibrium isotherm, kinetics and thermodynamics of interactions. *Desalination* **261**(1–2), 52–60. https://doi.org/10.1016/j.desal.2010.05.032.

Li, Z., Chen, K., Chen, Z., Li, W., Biney, B. W., Guo, A. & Liu, D. 2021 Removal of malachite green dye from aqueous solution by adsorbents derived from polyurethane plastic waste. *Journal of Environmental Chemical Engineering* **9**(1), 104704. https://doi.org/10.1016/j.jece.2020.104704.

Lin, L., Tang, S., Wang, X., Sun, X. & Yu, A. 2020 Adsorption of malachite green from aqueous solution by nylon microplastics: reaction mechanism and the optimum conditions by response surface methodology. *Process Safety and Environmental Protection* **140**, 339–347. https://doi.org/10.1016/j.psep.2020.05.019.

Mahanta, D., Madras, G., Radhakrishnan, S. & Patil, S. 2009 Adsorption and desorption kinetics of anionic dyes on doped polyaniline. *The Journal of Physical Chemistry. B.* **113**(8), 2293–2299. https://doi.org/10.1021/jp809796e.

Mahmoud, M. E., Amira, M. F., Seleim, S. M. & Mohamed, A. K. 2017 Adsorption isotherm models, kinetics study, and thermodynamic parameters of Ni(II) and Zn(II) removal from water using the LbL technique. *Journal of Chemical & Engineering Data* **62**(2), 839–850. https://doi.org/10.1021/acs.jced.6b00865.

Melo, R. P. F., Barros Neto, E. L., Moura, M. C. P. A., Castro Dantas, T. N., Dantas Neto, A. A. & Oliveira, H. N. M. 2014 Removal of Reactive Blue 19 using nonionic surfactant in cloud point extraction. *Separation and Purification Technology* **138**, 71–76. https://doi.org/10.1016/j.seppur.2014.10.009.

Melo, R. P. F., Barros Neto, E. L., Moura, M. C. P. A., Castro Dantas, T. N., Dantas Neto, A. A. & Oliveira, H. N. M. 2015 Removal of direct Yellow 27 dye using animal fat and vegetable oil-based surfactant. *Journal of Water Process Engineering* **7**, 196–202. https://doi.org/10.1016/j.jwpe.2015.06.009.

Melo, R. P. F., Barros Neto, E. L., Moura, M. C. P. A., Castro Dantas, T. N., Dantas Neto, A. A. & Nunes, S. K. S. 2017 Removal of direct Yellow 27 dye by ionic flocculation: the use of an environmentally friendly surfactant. *Journal of Surfactants and Detergents* **20**, 459–465. https://doi.org/10.1007/s11743-497016-1913-9.

Mohammed, N., Grishkewich, N., Berry, R. M. & Tam, K. C. 2015 Cellulose nanocrystal–alginate hydrogel beads as novel adsorbents for organic dyes in aqueous solutions. *Cellulose* **22**(6), 3725–3738. http://dx.doi.org/10.1007/s10570-015-0747-3.

Nascimento, R. F., Lima, A. C. A., Vidal, C. B., Melo, D. Q. & Raulino, G. S. C. 2020 *Adsorption: Theoretical Aspects and Environmental Applications*. UFC Publisher, Brazil.

Noïk, C., Bavière, M. & Defives, D. 1987 Anionic surfactant precipitation in hard water. *Journal of Colloid and Interface Science* **115**(1), 36–45. https://doi.org/10.1016/0021-9797(87)90006-3.

Oyelude, E. O., Awudza, J. A. M. & Twumasi, S. K. 2018 Removal of malachite green from aqueous solution using pulverized teak leaf litter: equilibrium, kinetic and thermodynamic studies. *Chemistry Central Journal* **12**(1), 1–10. https://doi.org/10.1186/s13065-018-0448-8.

Ozacar, M. & Sengil, A. 2005 Adsorption of metal complex dyes from aqueous solutions by pine sawdust. *Bioresource Technology* **96**(7), 791–795. https://doi.org/10.1016/j.biortech.2004.07.011.

Pan, X., Zuo, G., Su, T., Cheng, S., Gu, Y., Qi, X. & Dong, W. 2019 Polycarboxylic magnetic polydopamine sub-microspheres for effective adsorption of malachite green. *Colloids and Surfaces A: Physicochemical and Engineering Aspects* **560**, 106–113. https://doi.org/10.1016/j.colsurfa.2018.10.014.

Qu, W., Yuan, T., Yin, G., Xu, S., Zhang, Q. & Su, H. 2019 Effect of properties of active carbon on malachite green adsorption. *Fuel* **249**, 45–53. https://doi.org/10.1016/j.fuel.2019.03.058.

Rajabi, M., Mahanpoor, K. & Moradi, O. 2019 Preparation of PMMA/GO and PMMA/GO-Fe_3O_4 nanocomposites for malachite green dye adsorption: kinetic and thermodynamic studies. *Composites Part B* **167**, 544–555. https://doi.org/10.1016/j.compositesb.2019.03.030.

Ramesh, A., Hasegawa, W., Sugimoto, W., Maki, T. & Ueda, K. 2008 Adsorption of gold(III), platinum(IV), and palladium(II) onto glycine modified crosslinked chitosan resin. *Bioresource Technology* **99**(9), 3801–3809. https://doi.org/10.1016/j.biortech.2007.07.008.

Romero-Cano, L. A., Garcia-Rosero, H., Gonzalez-Gutierrez, L. V., Baldenegro-Pérez, L. A. & Carrasco-Marín, F. 2017 Functionalized adsorbents prepared from fruit peels: equilibrium, kinetic and thermodynamic studies for copper adsorption in aqueous solution. *Journal of Cleaner Production* **162**, 195–204. https://doi.org/10.1016/j.jclepro.2017.06.032.

Sadiq, A. C., Rahim, N. Y. & Suah, F. B. M. 2020 Adsorption and desorption of malachite green by using chitosan-deep eutectic solvents beads. *International Journal of Biological Macromolecules* **164**, 3965–3973. https://doi.org/10.1016/j.ijbiomac.2020.09.029.

Salamat, S., Hadavifar, M. & Rezaei, H. 2019 Preparation of nanochitosan-STP from shrimp shell and its application in removing of malachite green from aqueous solutions. *Journal of Environmental Chemical Engineering* **7**(5), 103328. https://doi.org/10.1016/j.jece.2019.103328.

Sharifpour, E., Dil, E. A., Asfaram, A., Ghaedi, M. & Goudarzi, A. 2019 Optimizing adsorptive removal of malachite green and methyl orange dyes from simulated wastewater by Mn- doped CuO- nanoparticles loaded on activated carbon using CCD-malachite green dye. *International Journal of Biological Macromolecules* **148**, 1130–1139. https://doi.org/10.1002/aoc.4768.

Sirianuntapiboon, S., Sadahiro, O. & Salee, P. 2007 Some properties of granular active carbon-sequencing batch reactor (GAC-SBR) system for treatment of textile wastewater containing direct dyes. *Journal of Environmental Management* **85**(1), 162–170. https://doi.org/10.1016/j.jenvman.2006.09.001.

Srivastava, S. J., Gupta, A. K., Srivastava, P. K. & Abhinav, A. 2004 Acute toxicity of malachite Green to fingerlings of common carp, Cyprinus carpio. *Biological Memoirs* **30**(2), 120–121.

Stellner, K. L. & Scamehorn, J. F. 1989 Hardness tolerance of anionic surfactant solution. 1. Anionic surfactant with added monovalent electrolyte. *Langmuir* **5**(1), 70–77. https://doi.org/10.1021/la00085a014.

UCCC (University of California Committee of Consultants) 1974 *Guidelines for Interpretations of Water Quality for Irrigation*. Technical Bulletin, University of California Committee of Consultants, California, USA, pp. 20–28.

Verma, A. K., Dash, R. R. & Bhunia, P. 2012 A review on chemical coagulation/flocculation technologies for removal of colour from textile wastewaters. *Journal of Environmental Management* **93**(1), 154–168. https://doi.org/10.1016/j.jenvman.2011.09.012.

Verma, A., Thakur, S., Mamba, G., Prateek, Gupta, R. K., Thakur, P. & Thakur, V. K. 2020 Graphite modified sodium alginate hydrogel composite for efficient removal of malachite green dye. *International Journal of Biological Macromolecules* **148**, 1130–1139. https://doi.org/10.1016/j.ijbiomac.2020.01.142.

Weber, W. J. 1984 Evolution of a technology. *Journal of Environmental Engineering* **110**, 899–917. https://doi.org/10.1061/(ASCE)0733-9372(1984)110:5(899).

White, R. L., White, C. M., Turgut, H., Massoud, A. & Tian, Z. R. 2018 Comparative studies on copper oxide adsorption of graphene and functionalized graphene oxide nanoparticles. *Journal of the Taiwan Institute of Chemical Engineers* **85**, 18–28. https://doi.org/10.1016/j.jtice.2018.01.036.

Wong, Y. C., Szeto, Y. S., Cheung, W. & McKay, G. 2003 Equilibrium studies for acid dye adsorption on chitosan. *Langmuir* **19**(19), 7888–7894. https://doi.org/10.1021/la030064y.

Wu, F. C., Tseng, R. L. & Juang, R. S. 2005 Comparisons of porous and adsorption properties of carbons activated by steam and KOH. *Journal of Colloid and Interface Science* **283**(1), 49–56. https://doi.org/10.1016/j.jcis.2004.08.037.

Xie, Y., Huang, J., Dong, H., Wu, T., Yu, L., Liu, G. & Yu, Y. 2020 Insight into performance and mechanism of tea polyphenols and ferric ions on reductive decolorization of malachite green cationic dye under moderate conditions. *Journal of Environmental Management* **261**, 110226. https://doi.org/10.1016/j.jenvman.2020.110226.

Zhang, H., Zhang, F. & Huang, Q. 2017 Highly effective removal of malachite green from aqueous solution by hydrochar derived from phycocyaninextracted algal bloom residues through hydrothermal carbonization. *RSC Advances* **7**(10), 5790–5799. https://doi.org/10.1039/C6RA27782A.

First received 17 February 2022; accepted in revised form 12 May 2022. Available online 19 May 2022